First principles simulation of amorphous InSb

Jan H. Los and Thomas D. Kühne*
Institute of Physical Chemistry and Center for Computational Sciences, Johannes Gutenberg University Mainz, Staudinger Weg 7, D-55128 Mainz, Germany

Silvia Gabardi and Marco Bernasconi†
Dipartimento di Scienza dei Materiali, Università di Milano-Bicocca, Via R. Cozzi 53, I-20125 Milano, Italy
(Received 15 January 2013; published 7 May 2013)

Ab initio molecular dynamics simulations based on density functional theory have been performed to generate a model of amorphous InSb by quenching from the melt. The resulting network is mostly tetrahedral with a minor fraction (10%) of atoms in a fivefold coordination. The structural properties are in good agreement with available x-ray diffraction and extended x-ray-absorption fine structure data and confirm the proposed presence of a sizable fraction of homopolar In-In and Sb-Sb bonds whose concentration in our model amounts to about 20% of the total number of bonds.

DOI: 10.1103/PhysRevB.87.184201 PACS number(s): 61.43.Bn

I. INTRODUCTION

Amorphous semiconductors are of special interest because of their omnipresence in a large variety of different micro- and optoelectronic devices. In particular, amorphous InSb (a-InSb) is investigated for applications in infrared photodetectors[1] and, at the eutectic composition, as a phase change material in a rewritable digital versatile disk (DVD).[2] A systematic x-ray diffraction study of the structural properties of amorphous III-V semiconductors, including InSb, has been performed long ago by Shevchik and Paul.[3] More recently, extended x-ray absorption fine structure (EXAFS) measurements revealed the presence of slightly longer bonds in a-InSb with respect to the crystal that is accompanied by a counterintuitive increase in density.[4] This feature has been ascribed to the presence of homopolar Sb-Sb and In-In bonds.[4] A sizable fraction of homopolar bonds is indeed present in models of a-InSb generated by quenching from the melt within classical molecular dynamics simulations using empirical interatomic potentials.[5,6] First principles simulations based on density functional theory (DFT) have been performed for both the liquid phase and a continuous random network model[7] of the amorphous phase.[8] A DFT atomistic model of a-InSb generated from the melt is, however, still lacking.

In this work, we present an analysis of the structural, electronic, and vibrational properties of a model of a-InSb generated from the liquid phase by means of DFT-based molecular dynamics simulations. The results are in good agreement with existing experimental data and confirm the presence of a sizable fraction of homopolar bonds. This analysis is also of interest as a preliminary work for future studies of InSb-based ternary compounds with phase change properties of interest for applications in nonvolatile data storage.[9]

II. COMPUTATIONAL METHODS

The amorphous model was generated by quenching from the melt within DFT-based *ab initio* molecular dynamics (AIMD) simulations by using the scheme of Kühne *et al.*.[10] In the spirit of the Car-Parrinello (CP)[11] approach the wave functions are not self-consistently optimized during the dynamics. However, in contrast to CP, large integration time steps can be used in the simulation. This scheme leads to a slightly dissipative dynamics of the type $-\gamma_D \dot{\mathbf{R}}_I$, where $\mathbf{R}_I$ are the ionic coordinates. In Refs. 10 and 12 it is shown how to compensate for this dissipation and obtain a correct canonical sampling. This scheme is implemented in the CP2K suite of programs.[13,14] We used the generalized gradient approximation to the exchange-correlation functional proposed by Perdew-Burke-Ernzerhof (PBE).[15] Goedecker-type pseudopotentials[16] with three and five valence electrons were adopted for In and Sb, respectively. The pseudopotentials were checked by computing the equation of state at zero temperature of the zinc-blende crystal with the QUANTUM-ESPRESSO[17] suite of programs and a $16 \times 16 \times 16$ Monkhorst-Pack mesh[18] for the integration of the Brillouin zone. The resulting equilibrium lattice parameter and bulk modulus are 6.62 Å and 34.6 GPa to be compared with the experimental values of 6.48 Å and 48.3 GPa.[19] This somehow large discrepancy with experiment in the lattice constant is also found in other DFT-PBE calculations using different codes and pseudopotentials.[20] In the AIMD simulations, the Kohn-Sham orbitals were expanded in a double-zeta valence plus polarization Gaussian-type basis set,[21] while the charge density has been expanded in a plane-wave basis set with a cutoff of 100 Ry to efficiently solve the Poisson equation within periodic boundary conditions using the Quickstep scheme.[13,14] Brillouin zone integration was restricted to the supercell Γ point. The same scheme was applied in our previous works on chalcogenide amorphous alloys.[22–29]

In order to better reproduce the band gap, the electronic density of states were calculated from Kohn-Sham (KS) energies using the Heyd-Scuseria-Ernzerhof (HSE) hybrid functional[30] on geometries optimized with the computationally less demanding PBE functional.

III. RESULTS

The amorphous phase was modeled by a cubic cell containing 216 atoms. The model was generated by first equilibrating

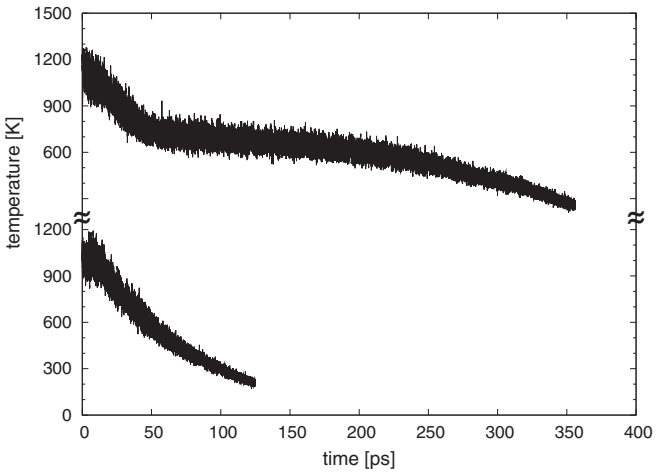

FIG. 1. Temperature as a function of time in the slow (upper curve) and fast (lower curve) quenching protocols.

the liquid phase above the melting point and then by quenching the model from 1000 to 300 K in 330 ps. The density was fixed to that of the crystalline phase of 0.0294 atoms/Å^3 (5.78 g/cm^3) as in previous molecular dynamics simulations with classical interatomic potentials.[5] In our previous works on the chalcogenide alloys GeTe (Ref. 29) and $Ge_2Sb_2Te_5$ (Ref. 22) the amorphous models were generated by quenching from the melt in about 80 ps. For GeTe we also checked that increasing the quenching time to 300 ps (Ref. 31) and even to 3 ns does not induce sizable changes in the structure of the amorphous. On the contrary, in InSb the long quenching time of 330 ps turned out to be mandatory. A faster quenching of 130 ps yielded amorphous models which were too similar to the liquid and contained only a small fraction of tetrahedra, while as discussed hereafter, the bonding network of the slowly quenched model is mostly tetrahedral. The evolution in time of the temperature in the fast and slow quenching protocols is reported in Fig. 1. The theoretical equilibrium density of the amorphous model generated by quenching from the melt was then obtained from a Murnaghan fitting of the energy-volume data of the optimized geometries at zero temperature. The resulting theoretical equilibrium density is 0.0286 atoms/Å^3 (5.61 g/cm^3). An experimental density of as-deposited amorphous InSb of 6.1 g/cm^3 (0.0311 atoms/Å^3) has been recently measured by x-ray reflectivity.[4] The resulting increase in density of about 5% with respect to the crystal is accompanied by a counterintuitive bond elongation of about 1%. These features have been ascribed in Ref. 4 to the presence of a large fraction of longer homopolar Sb-Sb and In-In bonds in the amorphous phase. The misfit of about 8% between the experimental density of a-InSb and that of our optimized amorphous model is not surprising if we consider that the theoretical DFT-PBE equilibrium density of the crystal is 6.6% lower than the experimental value (cf. Sec. II). An overestimation of the bond lengths using the PBE functional is actually also found in the Sb-containing amorphous compounds $Ge_2Sb_2Te_5$ (Ref. 22) and Sb_2Te_3.[26] The different preparation conditions of the amorphous phase, as-deposited in the experimental film and quenched from the melt in the simulations, might also be a source of deviation in the density. Anyway, in order to compare our structure with the recent EXAFS data,[4] the amorphous model at the density of 5.78 g/cm^3 was compressed up to the experimental density of 6.1 g/cm^3 by isotropically shrinking the simulation cell in a few steps. This is valid under the assumption that the misfit with experiments in the density is due to an error in the bond length and not to a difference in the topology of the amorphous network. Our model scaled at the experimental density is subject to a pressure of 1.2 GPa with a maximum off-diagonal component of the stress tensor of 0.13 GPa and a maximum anisotropy in the diagonal components of 0.26 GPa. The structural properties of the models at the two densities of 5.78 and 6.1 g/cm^3 are actually very similar as discussed below.

Structural properties. The total and partial correlation functions, reported in Fig. 2, are defined by

$$g_{\alpha\beta}(r) = \frac{1}{N_\alpha \rho_\beta} \sum_{I\in\alpha, J\in\beta} \langle \delta(\mathbf{r} + \mathbf{R}_I - \mathbf{R}_J) \rangle, \qquad (1)$$

where N_α is the number of atoms of species α and ρ_β is the density of atoms of specie β. The total pair correlation function is in turn given by

$$g(r) = \sum_{\alpha\beta} x_\alpha x_\beta g_{\alpha\beta}(r), \qquad (2)$$

where x_α is the number concentration of species α.[32] The average $\langle \cdots \rangle$ in Eq. (1) is computed over a 20-ps-long

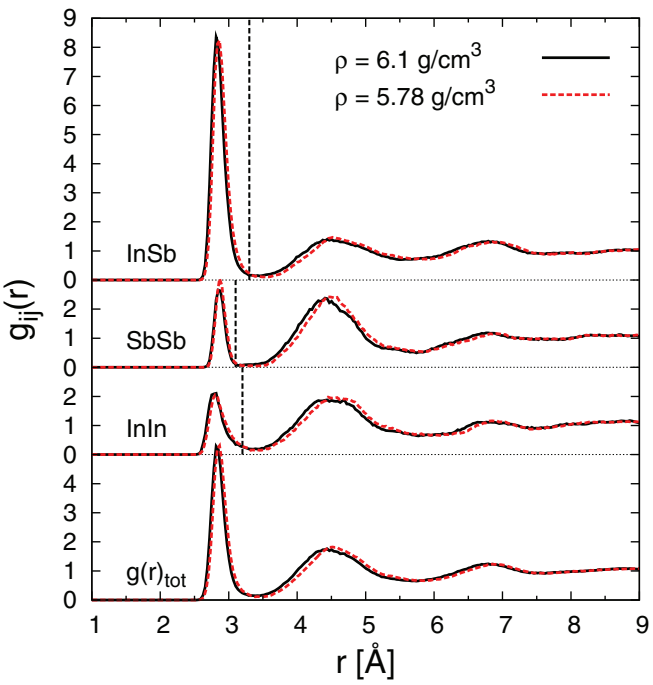

FIG. 2. (Color online) Total and partial pair correlation functions of amorphous InSb averaged over a 20-ps-long AIMD simulation at 300 K. The vertical lines are the bonding cutoff used to define the coordination numbers (3.20, 3.30, and 3.10 Å for the In-In, In-Sb, and Sb-Sb bonds, respectively). The maxima of the pair correlation functions are 2.82, 2.82, and 2.85 Å for the In-In, In-Sb, and Sb-Sb pairs. Results for the two models at the densities of 5.78 and 6.1 g/cm^3 are compared.

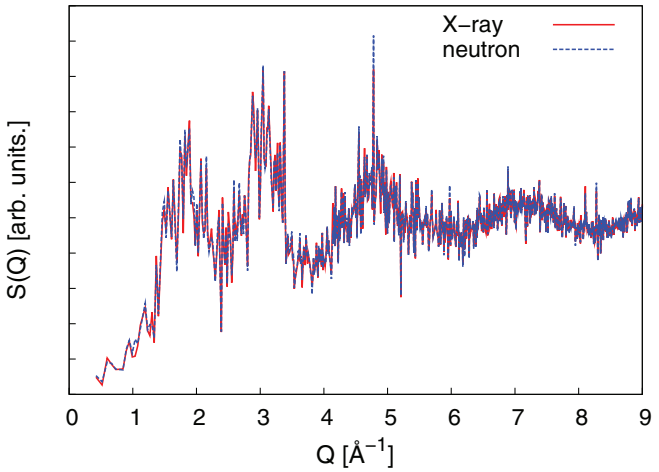

FIG. 3. (Color online) Structure factor of amorphous InSb at the density of 6.1 g/cm^3.

microcanonical AIMD run corresponding to an average temperature of 300 K. Results for the two models at the densities of 5.78 and 6.1 g/cm^3 are compared in Fig. 2. In the following we report results for the model at the experimental density of 6.1 g/cm^3, if not specified otherwise.

The total structure factor is reported in Fig. 3 as defined by[32]

$$S(Q) = \frac{1}{N\langle f^2(Q)\rangle} \sum_{I,J} f_I(Q) f_J(Q) \exp\left[i\mathbf{Q}\cdot(\mathbf{R}_I - \mathbf{R}_J)\right], \tag{3}$$

where the indices I and J run over the N atoms in the supercell and f_I is the x-ray or neutron atomic form factor of the Ith atom at position $\mathbf{R}_I$.

Average coordination numbers for the different species are given in Table I and the distribution of coordination numbers is reported in Fig. 4. The cutoff in the bonding distances used to define the coordination numbers are reported in Fig. 2.

The first peak in the total pair correlation function is at 2.82 Å, close to the experimental value of 2.86 Å in early x-ray diffraction measurements[3] and in even better agreement with the value of 2.826(5) Å obtained from recent EXAFS data.[4] The excellent agreement with the EXAFS data might be partially fortuitous due to the ∼2% overestimation of the lattice parameter of the crystal in the PBE calculation (cf. Sec. II). Still, in agreement with the conclusions of Ref. 4, we found that a large fraction of homopolar In-In and Sb-Sb bonds is present in a-InSb. This is shown by the height of the first peak in the partial pair correlation functions in Fig. 2 and

TABLE I. Average coordination numbers for different pairs of atoms computed from the partial pair correlation functions (cf. Fig. 2) for the model at the density of 6.1 g/cm^3. Data for the model at the density of 5.78 g/cm^3 are given in parentheses.

	With In	With Sb	Total
In	0.97 (0.92)	3.16 (3.14)	4.13 (4.06)
Sb	3.16 (3.14)	0.82 (0.83)	3.98 (3.96)

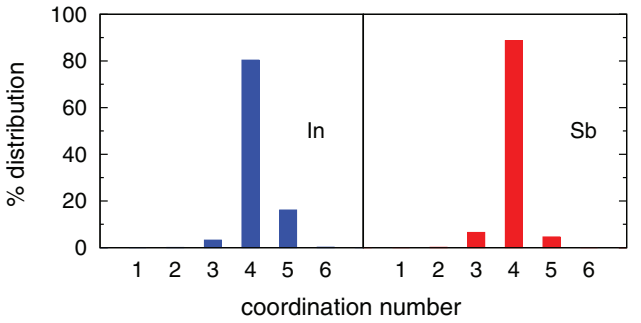

FIG. 4. (Color online) Distribution of the coordination numbers of amorphous InSb.

by the coordination numbers in Table I. About 12% of the total number of bonds are of In-In type, 10% of Sb-Sb type, and 78% of In-Sb type. The Sb-Sb bonds are slightly longer than In-Sb bonds, while In-In bonds are slightly shorter than In-Sb bonds (cf. Fig. 2). More than 80% of the atoms are fourfold coordinated as expected for the tetrahedral coordination. The distribution of the coordination environments is reported in Table II. Further insight on the local bonding geometry is gained from the angle distribution function in Fig. 5. The distribution is clearly peaked at the tetrahedral angle of 109.5°. An indicator of the tetrahedricity of the bonding geometry is given by the local order parameter q introduced in Ref. 33 and defined by $q = 1 - \frac{3}{8}\sum_{i>k}(\frac{1}{3} + \cos\theta_{ijk})^2$, where the sum runs over the pairs of atoms bonded to a central atom j and forming a bonding angle θ_{ijk}. The order parameter evaluates to $q = 1$ for the ideal tetrahedral geometry, to $q = 0$ for the six-coordinated octahedral site, and to $q = 5/8$ for a four-coordinated defective octahedral site. The distribution shown in Fig. 6 is peaked slightly below 1 as expected for a tetrahedral environment, but a long tail is present towards lower values indicating a sizable degree of deformation of the tetrahedra from the ideal geometry. The bonding properties in the different geometries is analyzed by computing the Wannier functions (WFs), which are the periodic version of the Boys orbitals obtained by the unitary transformation of the occupied KS orbitals that minimizes the quadratic spread.[34–36] The CPMD code[37] is used for this purpose. Isosurfaces of the WFs for selected local environments are shown in Fig. 7. The undercoordinated In atoms (threefold) are in part in a

TABLE II. Statistics of In and Sb coordination environments

	2	3	4	5
In:	1.8%	4.6%	76.9%	16.7%
	InSb: 0.9%	$InSb_2$: 3.7%	Sb_4: 33.3%	In_2Sb_3: 7.4%
	Sb_2: 0.9%	Sb_3: 0.9%	$InSb_3$: 32.4%	$InSb_4$: 4.6%
			In_2Sb_2: 9.3%	In_3Sb_2: 2.8%
			In_3Sb: 1.9%	In_4Sb: 0.9%
				Sb_5: 0.9%
Sb:		12.0%	69.4%	18.5%
		In_2Sb: 6.5%	In_4: 26.9%	In_5: 9.3%
		$InSb_2$: 3.7%	In_3Sb: 25.0%	In_4Sb: 8.3%
		Sb_3: 1.9%	In_2Sb_2: 16.7%	In_3Sb_2: 0.9%
			$InSb_3$: 0.9%	

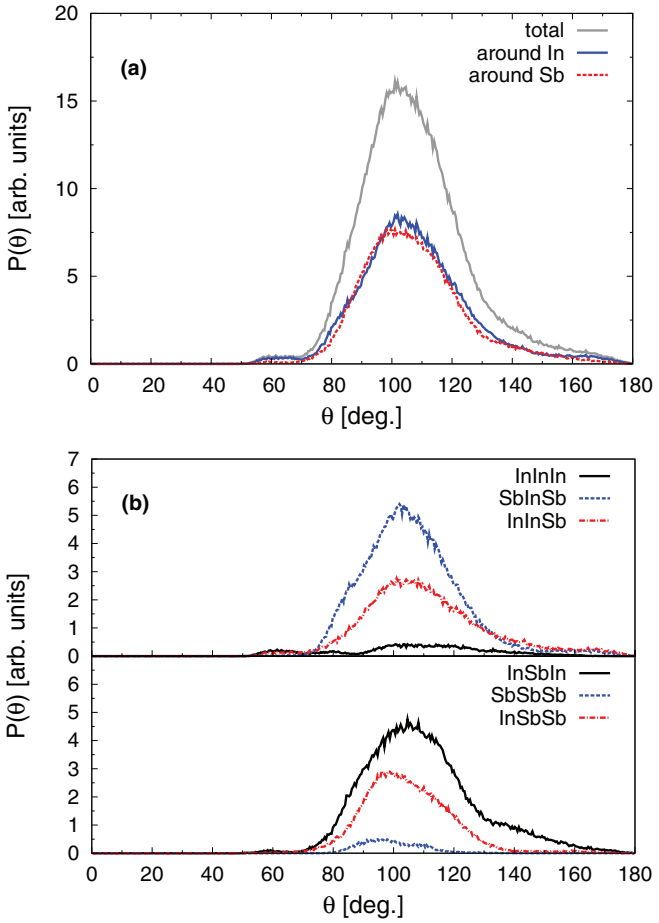

FIG. 5. (Color online) Bond angle distribution functions of a-InSb. (a) Total distribution around In and Sb. (b) Distribution resolved for the different triplets.

sp^2-like planar bonding geometry [Fig. 7(b)] and in part in a +1 oxidation state with an *s*-like lone pair. Most of the overcoordinated In atoms (fivefold) are in the trigonal bipyramid geometry shown in Fig. 7(c). The undercoordinated (threefold) Sb atoms are in a defective, octahedral-like geometry similar to those found in the phase change compounds Sb_2Te_3 (Ref. 26) and $Ge_2Sb_2Te_5$.[22] In this geometry, Sb forms three *p*-type bonds with the neighboring atoms, while the *s* electrons form a lone pair as demonstrated by the WFs in

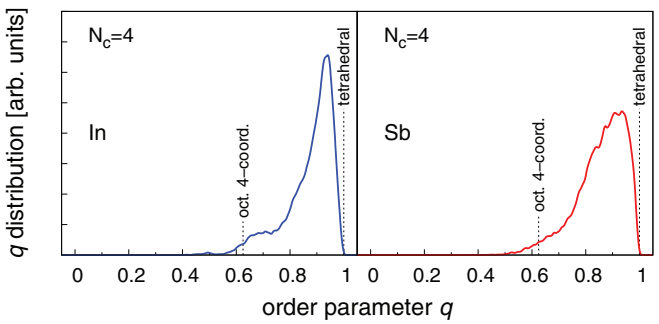

FIG. 6. (Color online) Distribution of the local order parameter *q* for tetrahedricity (see text) of fourfold coordinated In and Sb atoms. Vertical lines indicate the values of *q* for selected ideal geometries.

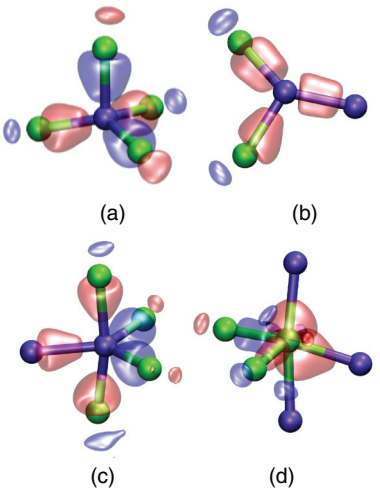

FIG. 7. (Color online) Isosurface of Wannier functions for (a) In in tetrahedral sites, (b) In in a planar sp^2-like configuration (threefold coordinated), (c) In in a trigonal bipyramid geometry (fivefold coordinated), and (d) Sb in defective octahedra (fivefold coordinated). Atoms of In are depicted by dark (violet) spheres and Sb by gray (green) spheres. Isosurfaces with different colors (red and blue) have different signs. Wannier functions with spherical isosurfaces in (d) are *s-type* lone pairs.

Fig. 7(d). Most of the overcoordinated (fivefold) Sb atoms are in defective octahedral geometry as well, but a fraction of them are in a trigonal bipyramid geometry similar to those formed by In.

Concerning the medium range order we report the distribution of rings length in Fig. 8 computed according to Ref. 38. The six-membered ring, typical of the crystalline zinc-blende structure, is the most abundant one also in the amorphous phase. However, a large fraction of five-membered and seven-membered rings is also present.

We remark that the various models obtained by quenching from the melt in about 130 ps, instead of 330 ps, are very different from that discussed above. Only about 40% of the atoms are fourfold coordinated with a large fraction of threefold coordinated atoms forming planar structures. Among the fourfold coordinated atoms a large fraction form defective octahedra. Tetrahedra are thus a minority

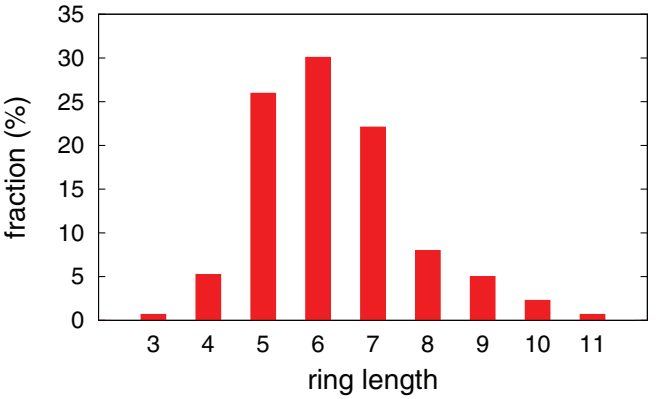

FIG. 8. (Color online) Ring distribution function of InSb computed according to Ref. 38.

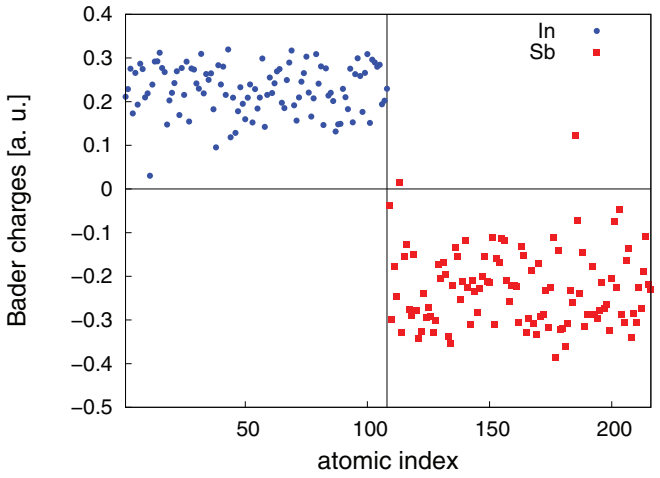

FIG. 9. (Color online) Bader ionic charges (atomic units) of a-InSb. Each point corresponds to an individual atom in the supercell.

fraction of the local bonding geometry. The same results were obtained for four independent models quenched from the melt with the same protocol and a quenching time of 80 ps from 1000 to 300 K. Relatively long quenching times are therefore needed to generate reliable amorphous models of a-InSb.

Electronic properties. To investigate the atomic oxidation state, we computed the Bader ionic charges from the total electronic charge density by using the scheme of Ref. 39. To this aim we added to the valence charge density the core charges localized on the atoms. The results reported in Fig. 9 show a tail of the distribution towards zero due to the presence of homopolar bonds.

The electronic density of states (DOS) of a-InSb is shown in Fig. 10 as computed from KS orbitals at the supercell Γ point broadened by a Gaussian function with a variance of 27 meV. The KS orbitals are computed with the HSE hybrid functional,[30] which better reproduces band gaps, by using the geometry optimized at the DFT-PBE level of theory. Projection of the DOS on atomic orbitals is also given in Fig. 10. The HSE highest occupied molecular orbital–lowest unoccupied molecular orbital (HOMO-LUMO) gap is 0.236 eV, while the HSE Tauc gap is 0.245 eV, a value slightly higher than the experimental optical Tauc gap of 0.15 (Ref. 40) or 0.17 eV.[41] To quantify the localization properties of individual KS states, we have computed the inverse participation ratio (IPR), which is defined for the ith KS state by $\sum_j c_{ij}^4/(\sum_j c_{ij}^2)^2$, where j runs over the Gaussian-type orbitals (GTOs) of the basis set, while c_{ij} are the expansion coefficients of the ith KS state in GTOs. The IPR is given in Figs. 10(a) and 10(b). Apparently, no localized states ascribed to defects can be found, either at the valence and conduction band edges, or in the band gap.

Vibrational properties. We computed the phonon frequencies of the amorphous model by diagonalizing the dynamical matrix obtained in turn from the variation of atomic forces due to finite atomic displacements 0.0053 Å large. Only phonons with the periodicity of our supercell (Γ-point phonons) were considered. The phonon density of states is shown in Fig. 11(a).

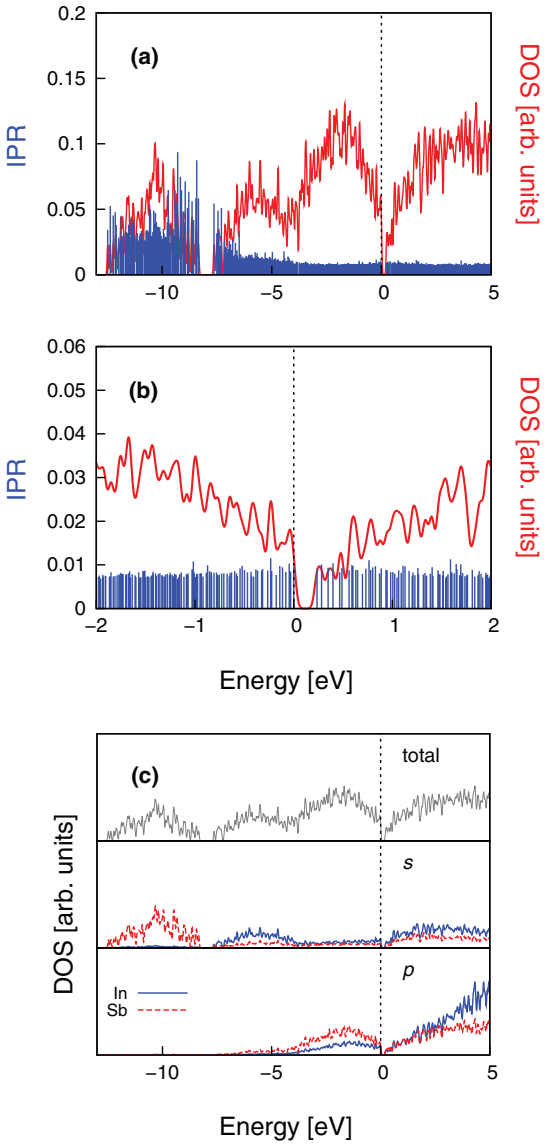

FIG. 10. (Color online) (a) Electronic density of states [HSE hybrid functional (Ref. 30)] of a-InSb. The KS energies are broadened by Gaussian functions of 27 meV width. The zero of energy corresponds to the top of the valence band. The IPR is given on the left scale (blue spikes; see text for definition). (b) A zooming of the DOS of panel (a) close to the band gap. (c) Projections of the DOS on atomic s and p pseudo wave functions. The contribution from d pseudo wave functions is negligible on the scale of the figure and is omitted.

In an amorphous material, phonons display localization properties that depend on the frequency. To address this issue, we have computed the IPR of the j th vibrational mode defined as

$$\mathrm{IPR} = \frac{\sum_\kappa \left| \frac{\mathbf{e}(j,\kappa)}{\sqrt{M_\kappa}} \right|^4}{\left(\sum_\kappa \frac{|\mathbf{e}(j,\kappa)|^2}{M_\kappa} \right)^2}, \tag{4}$$

where $\mathbf{e}(j,\kappa)$ are phonon eigenvectors, while the sum over κ runs over the N atoms in the unit cell with masses M_κ. According to this definition, the value of the IPR varies from $1/N$ for a completely delocalized phonon, to one for a mode

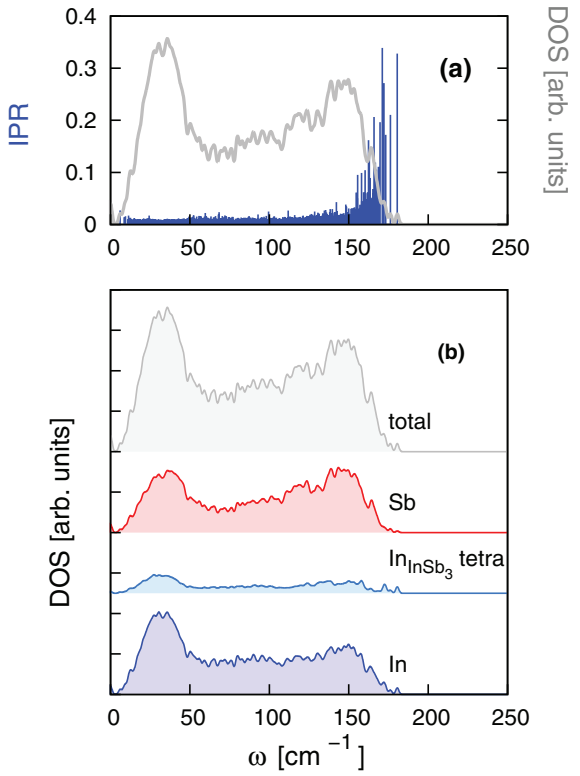

FIG. 11. (Color online) (a) Theoretical phonon DOS of a-InSb. The phonon IPR (blue spikes, left scale; see text for definition) is superimposed to the DOS. (b) Projections of the phonon DOS on different species (In and Sb) and on In atoms at the center of In-$InSb_3$ tetrahedra responsible for the strongly localized modes above 160 cm^{-1}.

completely localized on a single atom. The plot of the IPR in Fig. 11(b) reveals the presence of phonons strongly localized on In-$InSb_3$ tetrahedra above 160 cm^{-1}. To the best of our knowledge no experimental data to compare with is available for the phonon DOS of a-InSb.

IV. CONCLUSIONS

We have generated a model of amorphous InSb by quenching from the melt within DFT-based AIMD simulations. In the amorphous model most of the atoms are in a tetrahedral bonding geometry with a minority of about 17% of In atoms and 19% of Sb atoms in a fivefold coordination. Most of the overcoordinated In atoms are in a trigonal bipyramid configuration, while most of overcoordinated Sb atoms are in defective octahedra. The calculated pair correlation functions are in good agreement with experimental x-ray diffraction[3] and EXAFS[4] data. The results confirm the experimentally proposed[4] presence of a sizable fraction of homopolar In-In and Sb-Sb bonds, which in our model reaches the value of about 20% of the total number of bonds. However, since it actually turned out that a quenching time as long as 330 ps was necessary to get a mostly tetrahedral coordination, the resulting fraction of homopolar bonds might be slightly overestimated due to a still insufficient quenching protocol. The In-In homopolar bonds have fingerprints in the vibrational properties giving rise to phonons strongly localized on In-$InSb_3$ tetrahedral units above 160 cm^{-1}.

ACKNOWLEDGMENTS

J.L. and T.D.K. would like to acknowledge financial support form the IDEE project of the Carl-Zeiss Foundation and the Graduate School of Excellence MAINZ. S.G. and M.B. acknowledge funding from the European Union Seventh Framework Programme FP7/2007-2013 under grant agreement No. 310339.

*kuehne@uni-mainz.de
†marco.bernasconi@mater.unimib.it

[1] T. Zens, P. Becla, A. M. Agarwal, L. C. Kimerling, and A. Drehman, J. Cryst. Growth **334**, 84 (2011).
[2] E. Suzuki, H. Miura, M. Harigaya, K. Ito, N. Iwata, and A. Watada, Jpn. J. Appl. Phys. **44**, 3598 (2005).
[3] N. J. Shevchik and W. Paul, J. Non-Cryst. Solids **13**, 55 (1974).
[4] M. Krbal, A. V. Kolobov, B. Hyot, B. André, P. Fons, R. E. Simpson, T. Uruga, H. Tanida, and J. Tominaga, J. Appl. Phys. **108**, 023506 (2010).
[5] J. P. Rino, D. S. Borges, and S. C. Costa, J. Non-Cryst. Solids **348**, 17 (2004).
[6] J. P. Rino, P. S. Pizani, and S. C. Costa, Braz. J. Phys. **34**, 347 (2004).
[7] T. Gu, X. Bian, J. Qin, and C. Xu, Phys. Rev. B **71**, 104206 (2005).
[8] L. Wang, X. S. Chen, Y. Huang, W. Lu, and J. J. Zhao, Physica B **405**, 2481 (2010).
[9] M. Wuttig and N. Yamada, Nat. Mater. **6**, 824 (2007).
[10] T. D. Kühne, M. Krack, F. R. Mohamed, and M. Parrinello, Phys. Rev. Lett. **98**, 066401 (2007).
[11] R. Car and M. Parrinello, Phys. Rev. Lett. **55**, 2471 (1985).
[12] T. D. Kühne, M. Krack, and M. Parrinello, J. Chem. Theory Comput. **5**, 235 (2009).
[13] M. Krack and M. Parrinello, in *High Performance Computing in Chemistry*, edited by J. Grotendorst, NIC Vol. 25 (NIC-Directors, Juelich, 2004), pp. 29–51; www.cp2k.org.
[14] J. VandeVondele, M. Krack, F. Mohamed, M. Parrinello, T. Chassaing, and J. Hutter, Comput. Phys. Commun. **167**, 103 (2005).
[15] J. P. Perdew, K. Burke, and M. Ernzerhof, Phys. Rev. Lett. **77**, 3865 (1996).
[16] S. Goedecker, M. Teter, and J. Hutter, Phys. Rev. B **54**, 1703 (1996); M. Krack, Theor. Chem. Acc. **114**, 145 (2005).
[17] P. Giannozzi *et al.*, J. Phys.: Condens. Matter **21**, 395502 (2009); http://www.quantum-espresso.org.
[18] H. J. Monkhorst and J. D. Pack, Phys. Rev. B **13**, 5188 (1976).
[19] O. Madelung, *Numerical Data and Functional Relationships in Science and Technology* (Springer, Berlin, 1982).
[20] D. Toton, J. He, G. Gory, J. J. Kolodziej, S. Godlewski, L. Kantorovich, and M. Szymonski, J. Phys.: Condens. Matter **22**, 265001 (2010).
[21] J. VandeVondele and J. Hutter, J. Chem. Phys. **127**, 114105 (2007).
[22] S. Caravati, M. Bernasconi, T. D. Kühne, M. Krack, and M. Parrinello, Appl. Phys. Lett. **91**, 171906 (2007).

[23]S. Caravati, M. Bernasconi, T. D. Kühne, M. Krack, and M. Parrinello, Phys. Rev. Lett. **102**, 205502 (2009).
[24]S. Caravati, M. Bernasconi, T. D. Kühne, M. Krack, and M. Parrinello, J. Phys.: Condens. Matter **21**, 255501 (2009); **21**, 499803(E) (2009); **22**, 399801(E) (2010).
[25]S. Caravati, D. Colleoni, R. Mazzarello, T. D. Kühne, M. Krack, M. Bernasconi, and M. Parrinello, J. Phys.: Condens. Matter **23**, 265801 (2011).
[26]S. Caravati, M. Bernasconi, and M. Parrinello, Phys. Rev. B **81**, 014201 (2010).
[27]E. Spreafico, S. Caravati, and M. Bernasconi, Phys. Rev. B **83**, 144205 (2011).
[28]S. Gabardi, S. Caravati, M. Bernasconi, and M. Parrinello, J. Phys.: Condens. Matter **24**, 385803 (2012).
[29]R. Mazzarello, S. Caravati, S. Angioletti-Uberti, M. Bernasconi, and M. Parrinello, Phys. Rev. Lett. **104**, 085503 (2010); **107**, 039902(E) (2011).
[30]J. Heyd, G. E. Scuseria, and M. Ernzerhof, J. Chem. Phys. **118**, 8207 (2003); **124**, 219906(E) (2006).
[31]G. C. Sosso, G. Miceli, S. Caravati, J. Behler, and M. Bernasconi, Phys. Rev. B **85**, 174103 (2012).
[32]Y. Waseda, *The Structure of Non-Crystalline Materials* (McGraw-Hill, New York, 1980).
[33]J. R. Errington and P. G. Debenedetti, Nature (London) **409**, 318 (2001).
[34]N. Marzari and D. Vanderbilt, Phys. Rev. B **56**, 12847 (1997).
[35]P. L. Silvestrelli, N. Marzari, D. Vanderbilt, and M. Parrinello, Solid State Commun. **107**, 7 (1998).
[36]G. Berghold, C. J. Mundy, A. H. Romero, J. Hutter, and M. Parrinello, Phys. Rev. B **61**, 10040 (2000).
[37]http://www.cpmd.org/, copyright IBM Corp. 1990–2013, copyright MPI für Festkörperforschung Stuttgart (1997–2001).
[38]D. S. Franzblau, Phys. Rev. B **44**, 4925 (1991).
[39]G. Henkelman, A. Arnaldsson, and H. Jonsson, Comput. Math. Sci. **36**, 354 (2006).
[40]T. Ojima and S. Adachi, J. Appl. Phys. **82**, 3105 (1997).
[41]T. Dhawana, A. G. Vedeshwara, V. N. Singh, B. R. Mehta, and R. P. Tandon, Scr. Mater. **63**, 97 (2010).